Atmospheric
Chemistry
and Physics

Supplement of

Radiative forcing of anthropogenic aerosols on cirrus clouds using a hybrid ice nucleation scheme

Jialei Zhu and Joyce E. Penner

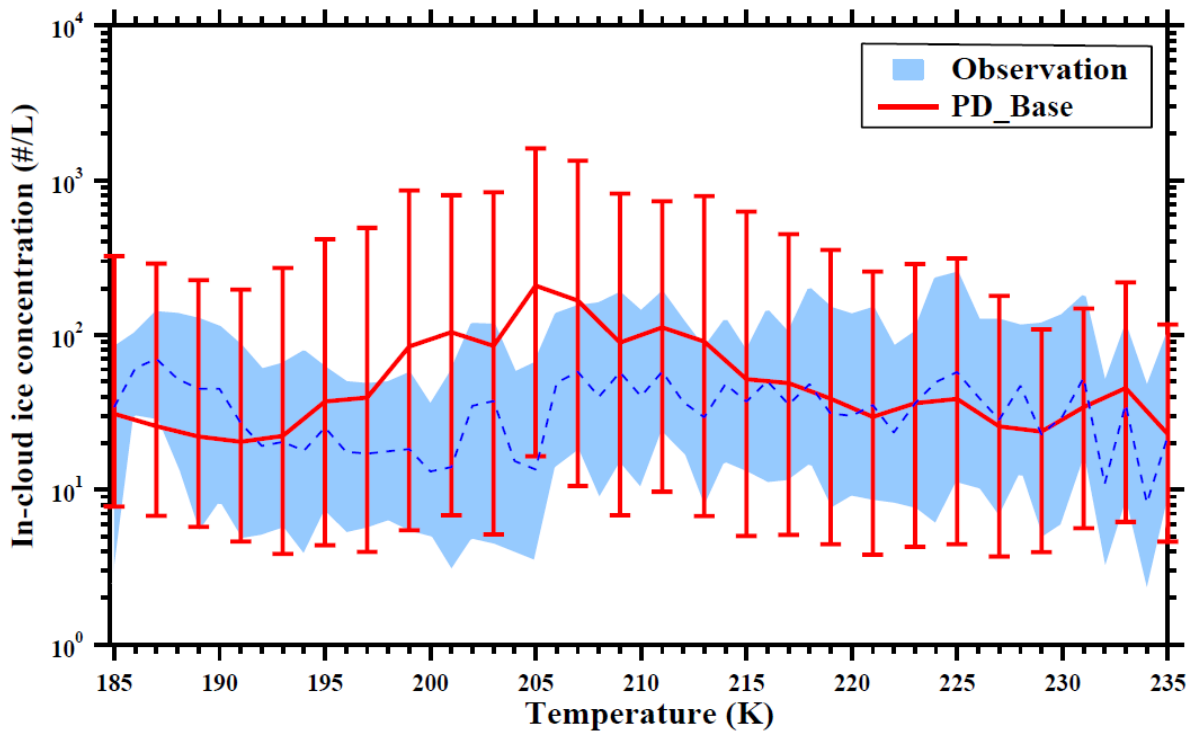*Correspondence to:* Jialei Zhu (zhujialei@tju.edu.cn)

Figure S1. The median of in-cloud ice crystal number concentration (red line) versus temperature from PD_Base case with error bars of 25th and 75th percentiles. The background shaded region shows the 25th-75th percentiles with the median value (blue dashed line) from a set of observations compiled by Krämer et al. (2009, 2020)
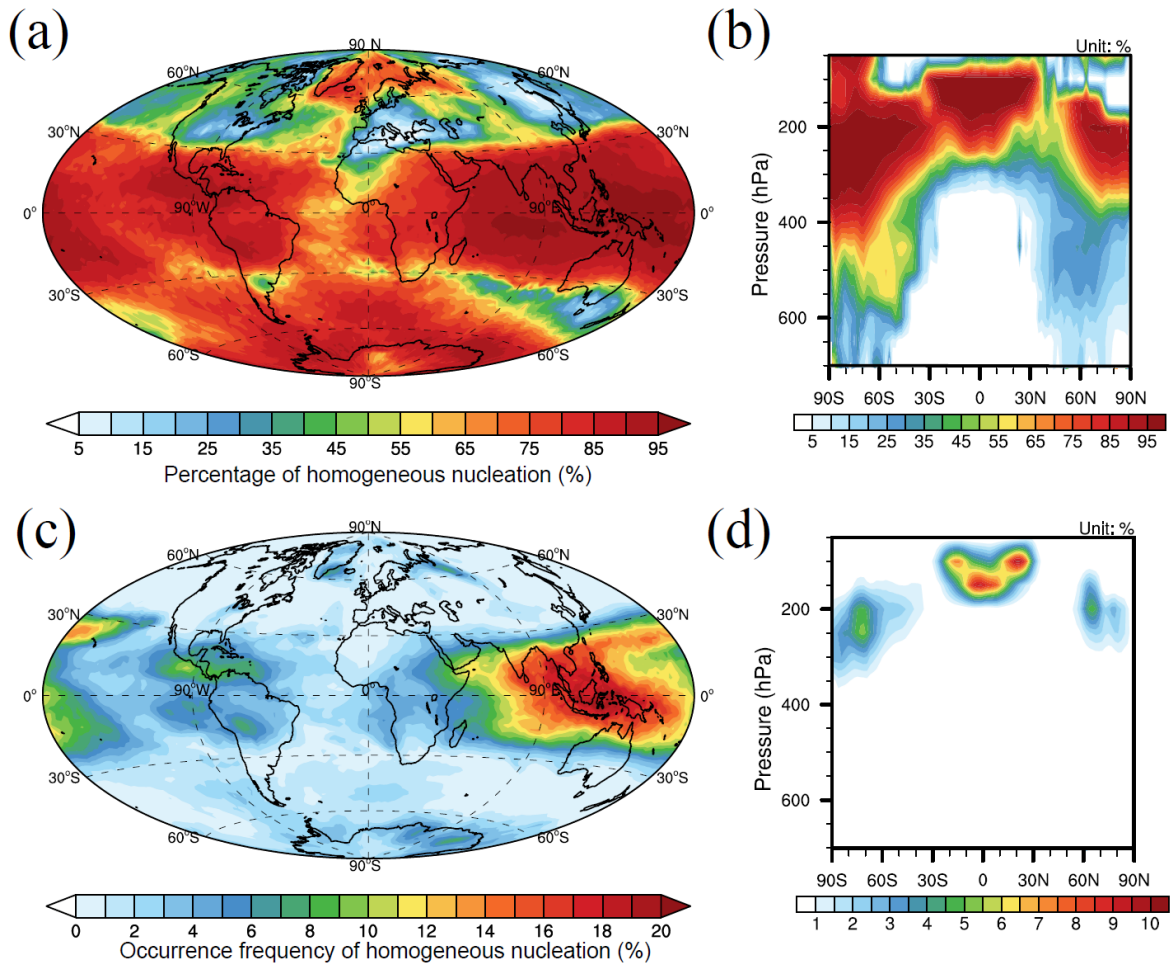
Figure S2. Vertically integrated percentage of new ice formed from homogeneous nucleation (a) and the cloud-weighed occurrence frequency of homogeneous nucleation (c) in the PD_Base case. The zonal average plots of percentage of new ice formed from homogeneous nucleation (b) and cloud-weighed occurrence frequency of homogeneous nucleation (d) in the PD_Base case.
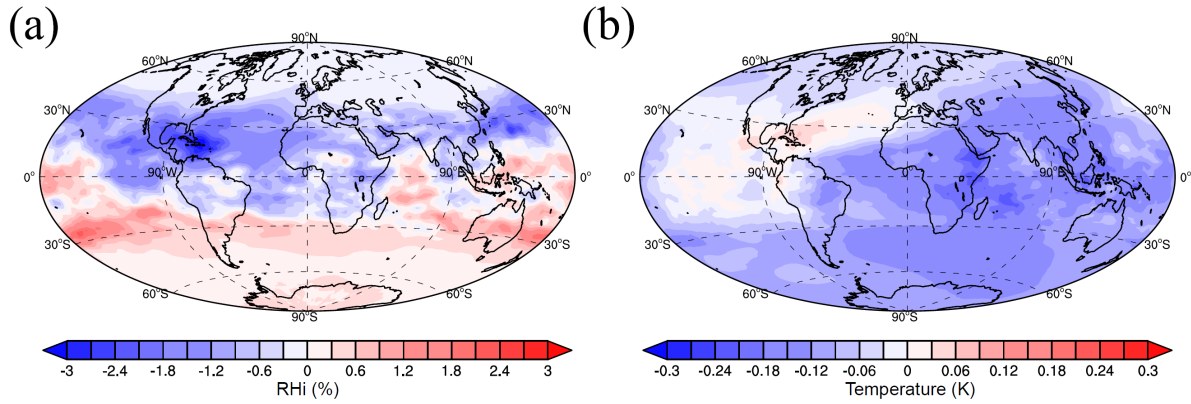
Figure S3. The annual average change in the RHi (a) and temperature (b) at 150 hPa for the difference between the PD_Base and PI_cSoot cases.
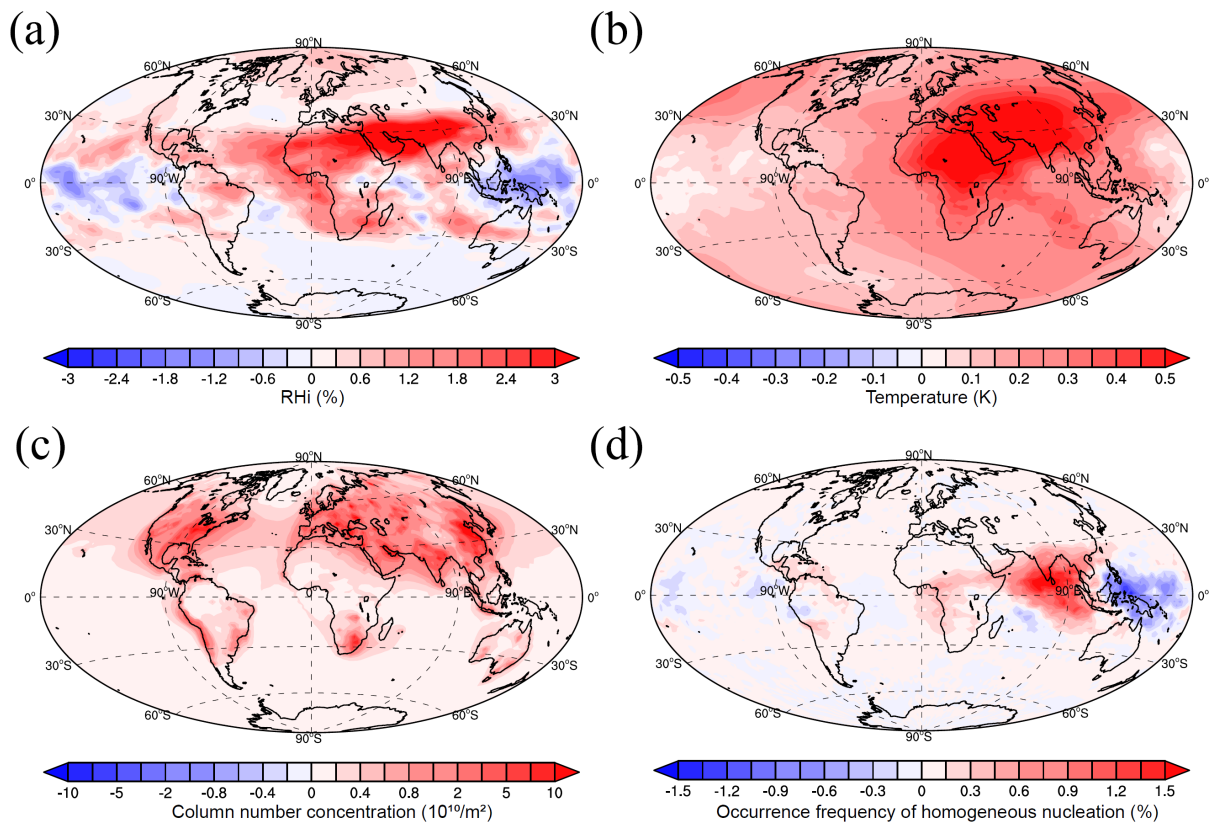
Figure S4. The annual average change in the RHi (a), temperature (b) and occurrence frequency of homogeneous nucleation (d) at 150 hPa as well as vertically integrated number concentration of sulfate in the Aitken and accumulation mode (c) for the difference between the PD_Base and PI_SO4 cases.

(a) MEAN=-0.19g/m²

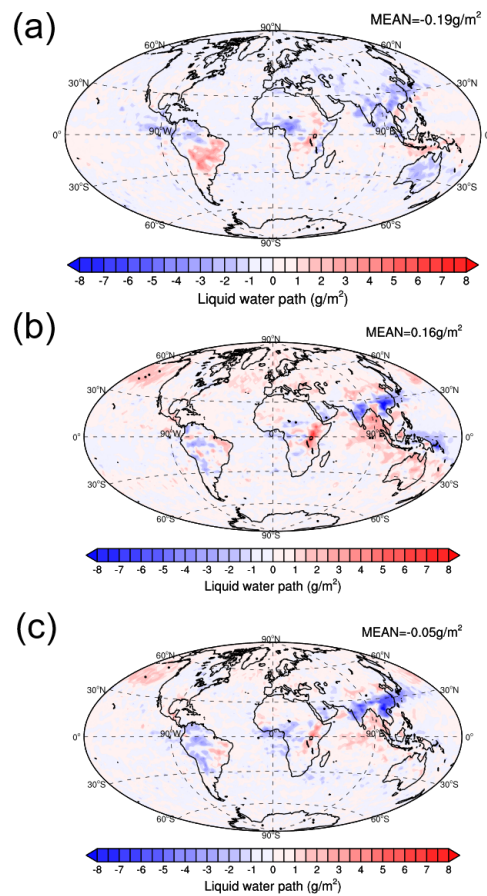(b) MEAN=0.16g/m²

(c) MEAN=-0.05g/m²

Figure S5. Annual mean plots of the change in vertically integrated averaged i liquid water path for the difference between the PD_Base and PI_cSoot cases (a,), PD_Base and PI_SO4 cases (b) as well as the PD_Base and PI_ALL cases (c). Differences significant at the 90% level according to a Student's t test are depicted by points.
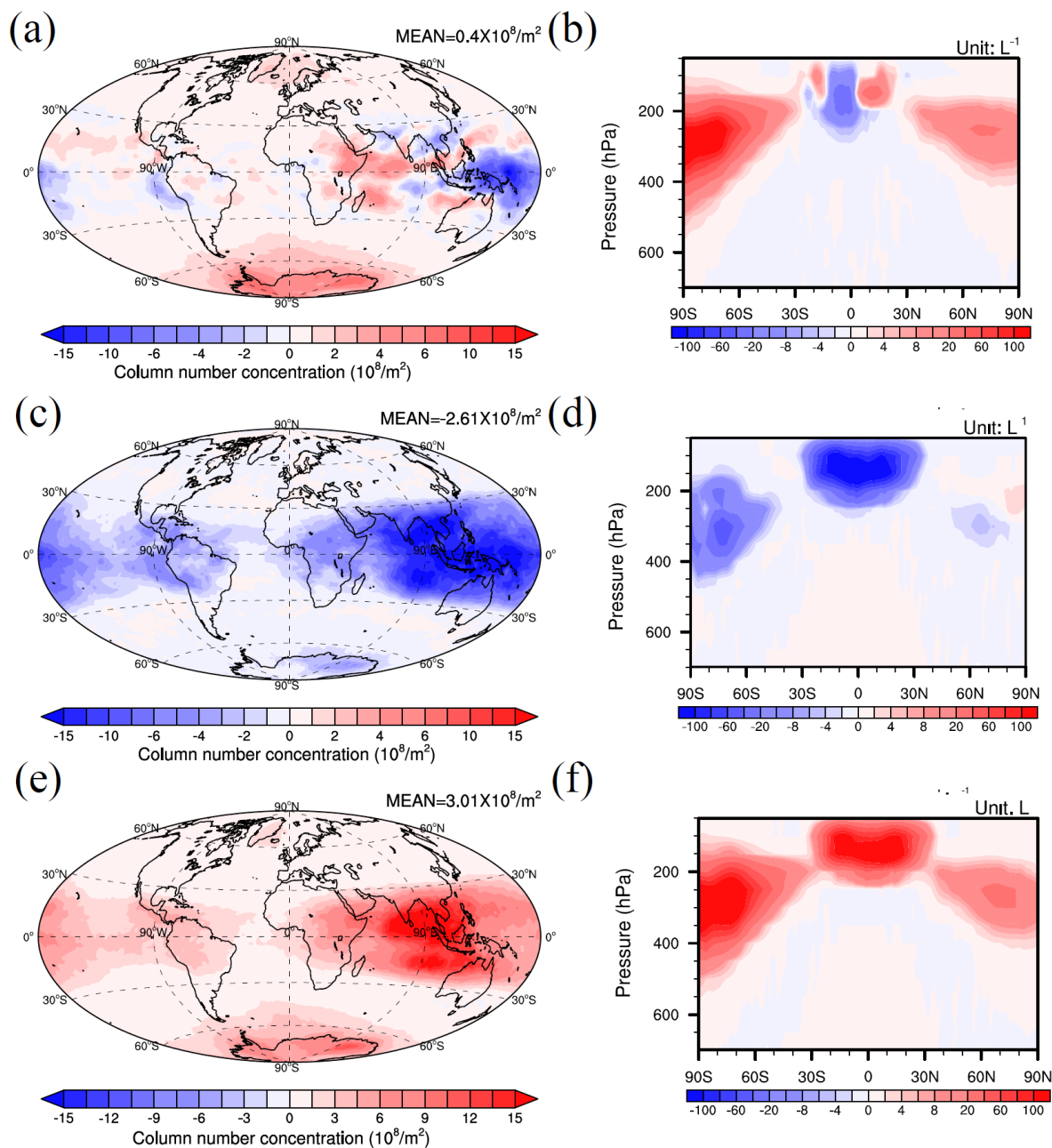
Figure S6. The annual average change in column number concentration (a, c, e) and zonal average number concentration (b, d, f) of total ice (a, b), ice from homogeneous nucleation (c, d) and ice from heterogeneous nucleation (e, f) for the difference between the PD_SOA and PD_Base cases. Differences significant at the 90% level of according to a Student's t test are depicted by points.

(a) MEAN=-0.31X10⁸/m²

(b) Unit: L⁻¹

(c) MEAN=-1.35X10⁸/m²

(d) Unit: L⁻¹

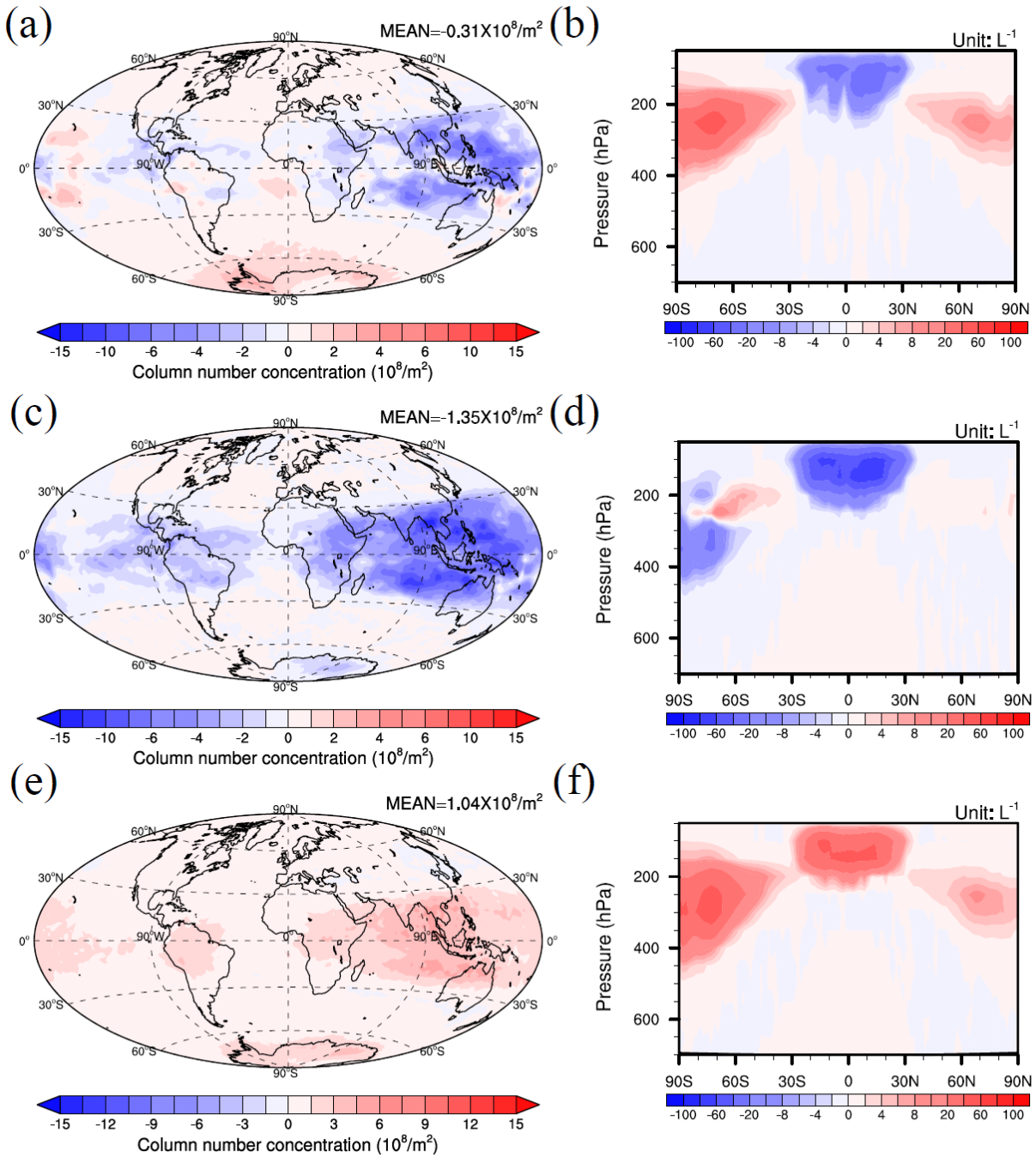**(e)** MEAN=1.04X10⁸/m²

(f) Unit: L⁻¹

Figure S7. As in Figure S6 but for the difference between the PI_SOA and PI_ALL cases. Differences significant at the 90% level according to a Student's t test are depicted by points.

Text S1 Sensitivity experiments with high concentration of INPs from dust

In order to examine the influence of heterogeneous nucleation on radiative forcing, sensitivity experiments with a high concentration of INPs from dust were conducted. In these experiments 100% of dust was assumed to act as an INP with all anthropogenic emissions for the present day (PD_HDust) and preindustrial periods (PI_HDust). In comparison, only dust with fewer than 3 monolayers of sulfate coating were assumed to act as INPs in PD_Base and PI_ALL cases. The global average Ni from heterogeneous nucleation is increased by about a factor of ~4 due to the high concentration of INPs from dust in PD_HDust case compared to PD_Base and there is a remarkable increase of Ni from heterogeneous nucleation in the main regions with dust sources like Sahara and Taklimakan as well as downwind from these regions (Figure S8b). In addition, homogeneous nucleation is inhibited by the increase in the INPs. The global average Ni from homogeneous nucleation is decreased by 27% in PD_HDust compared to PD_Base (Figure S8a). As a result, the assumption of 100% of dust acting as INPs increases Ni in the mid to high latitudes of the NH (30°N~90°N) where heterogeneous nucleation dominates, while Ni over the tropics is decreased due to the inhibition of homogeneous nucleation (Figure S9a). In total the global average Ni in the PD_HDust case is 11% lower that in the PD_Base case. The increased INPs from dust have a similar influence on Ni in the PI atmosphere, which leads to 12% lower global average Ni in the PI_HDust case than that in the PI_ALL case (Figure S9b). In this sensitivity experiment, Ni increases significantly in south Asia and the north Indian Ocean from the PI to PD atmosphere (Figure S10a, PD_HDust-PI_HDust), which is somewhat smaller than the increase in the base experiment (PD_Base-PI_ALL) due to the decrease in homogeneous nucleation. The decrease in Ni off the coast of east Asia from PI to PD in this sensitivity experiment is not as significant as that in base experiment (compare Figure S10a and Figure 5a) because the high concentration of INPs from

dust in the PI atmosphere leads to a smaller influence on Ni from anthropogenic emissions compared to the base experiment. As a result, the global average increase in Ni is somewhat larger from PI_HDust to PD_HDust (0.57×10^8 m^{-2}, Figure S10a) than the increase in base experiment (0.49×10^8 m^{-2}, Figure 5a).

The more positive change in Ni from PI to PD in this sensitivity experiment leads to a less negative change in the IWP than that in base experiment (compare Figure S10b and Figure 6e). Due to the larger change in Ni in this sensitivity experiment than that in the base experiment, the SRF is less positive (Figure S10c vs Figure 9a) and the LRF is less negative (Figure S10d vs Figure 9b) in the mid to high latitudes of the NH. SRF and LRF are smaller in south Asia and the north Indian Ocean in the sensitivity experiment compared to the base experiment. As a result, the NRF between PD_HDust and PI_HDust is -0.16 ± 0.06W m^{-2} (Figure S10e), which is less negative than the NRF in the base case (-0.20 ± 0.05W m^{-2}, Figure 9e). The increase in INPs from dust leads to a less negative NRF in the mid to high latitudes of the NH (30°N~90°N) and a less positive NRF between 20°N~30°N (Figure S10f).
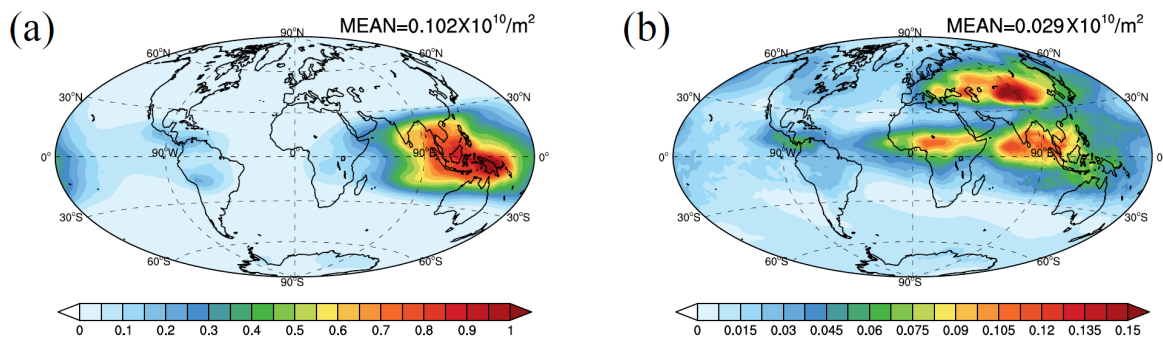
Figure S8. The vertically integrated *Ni* from homogeneous nucleation (a) and from heterogeneous nucleation (b) for the PD_HDust case.
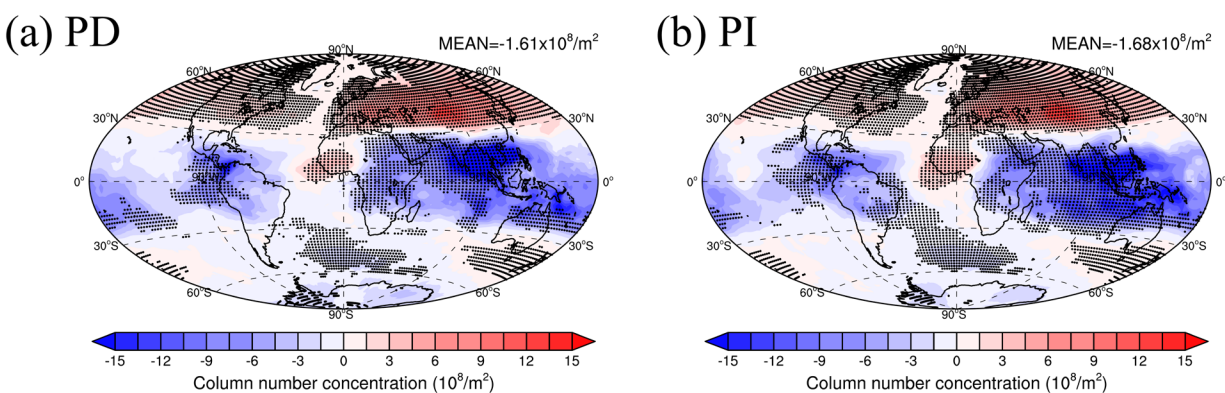

Figure S9. The difference in the column number concentration of Ni between PD_HDust and PD_Base (a) as well as PI_HDust and PI_ALL (b). Differences significant at the 90% level according to a Student's t test are depicted by points.
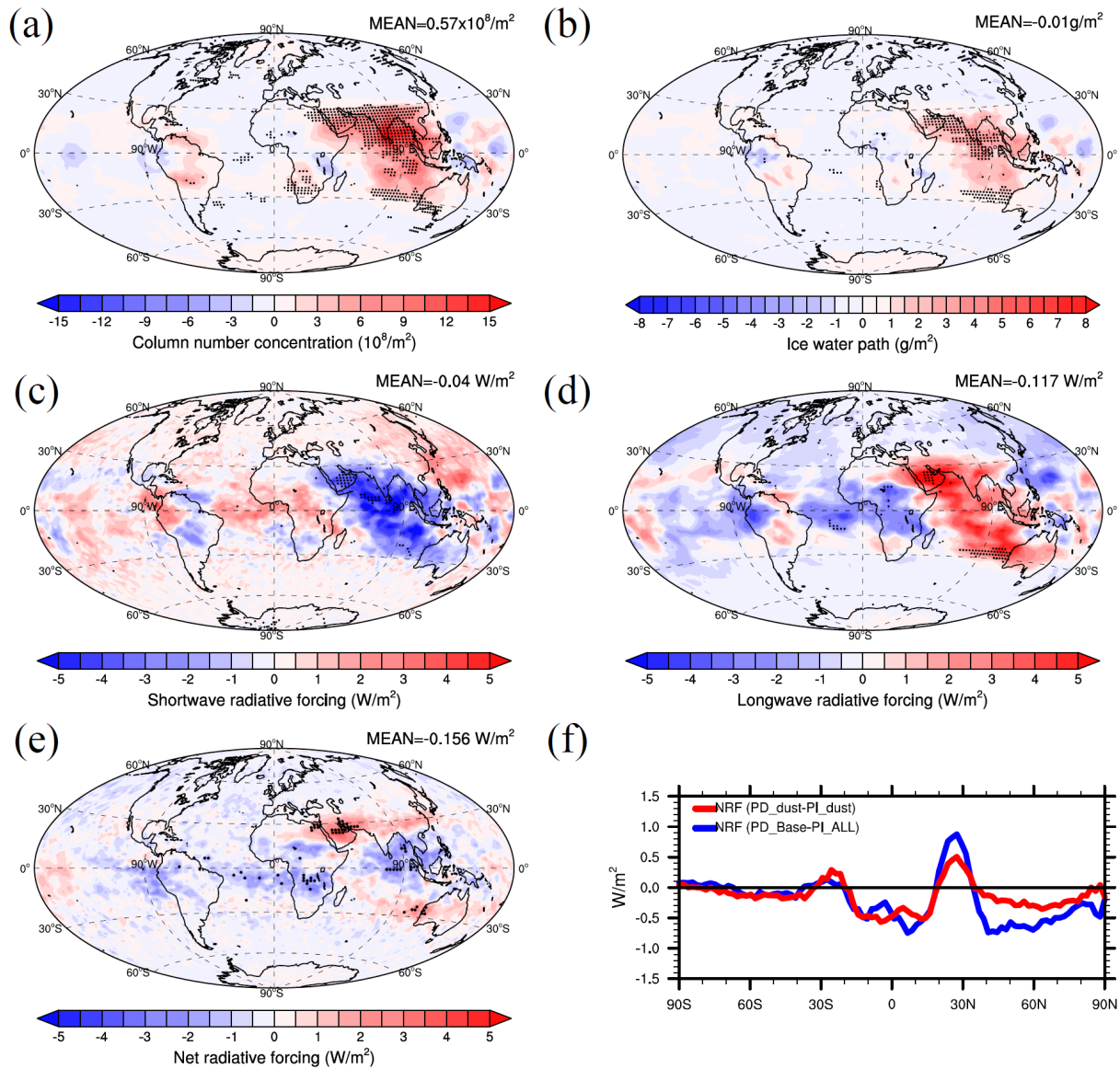
Figure S10. Annual mean plots of the changes in vertical integrated Ni (a), ice water path (b), shortwave radiative forcing (c), longwave radiative forcing (d), and all-sky net radiative forcing (e) as well as longwave radiative forcing (f, LRF, green dashed line), shortwave radiative forcing (f, SRF, blue dotted line) and all-sky net radiative forcing (f, NRF, red solid line) versus latitude for the difference between the PD_HDust and PI_HDust cases. Differences significant at the 90% level according to a Student's t test are depicted by points.